

Supplemental material for:

H3K27me3 dynamics dictate evolving uterine states in pregnancy and parturition

Patrice Nancy^{1*}, Johan Siewiera^{1,2*}, Gabrielle Rizzuto³, Elisa Tagliani¹, Ivan Osokine², Priyanka Manandhar², Igor Dolgalev¹, Caterina Clementi¹, Aristotelis Tsirigos¹, and Adrian Erlebacher^{1,2}

J Clin Invest. <https://doi.org/10.1172/JCI95937>

¹Department of Pathology, NYU School of Medicine, New York, New York USA

²Department of Laboratory Medicine, University of California San Francisco, San Francisco, CA, USA

³Department of Pathology, University of California San Francisco, San Francisco, California, USA

Corresponding author and present address: Department of Laboratory Medicine, University of California San Francisco, San Francisco, California, 94143, USA
Email: adrian.erlebacher@ucsf.edu

*Equal contributions

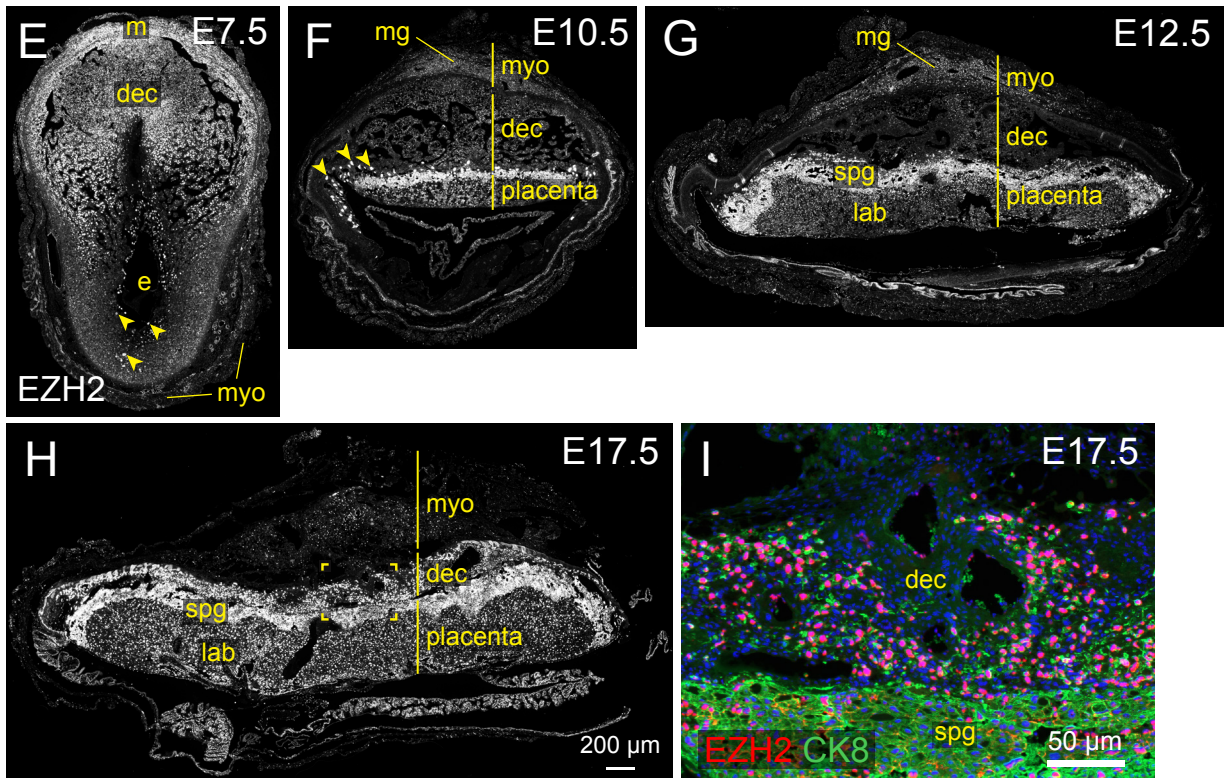
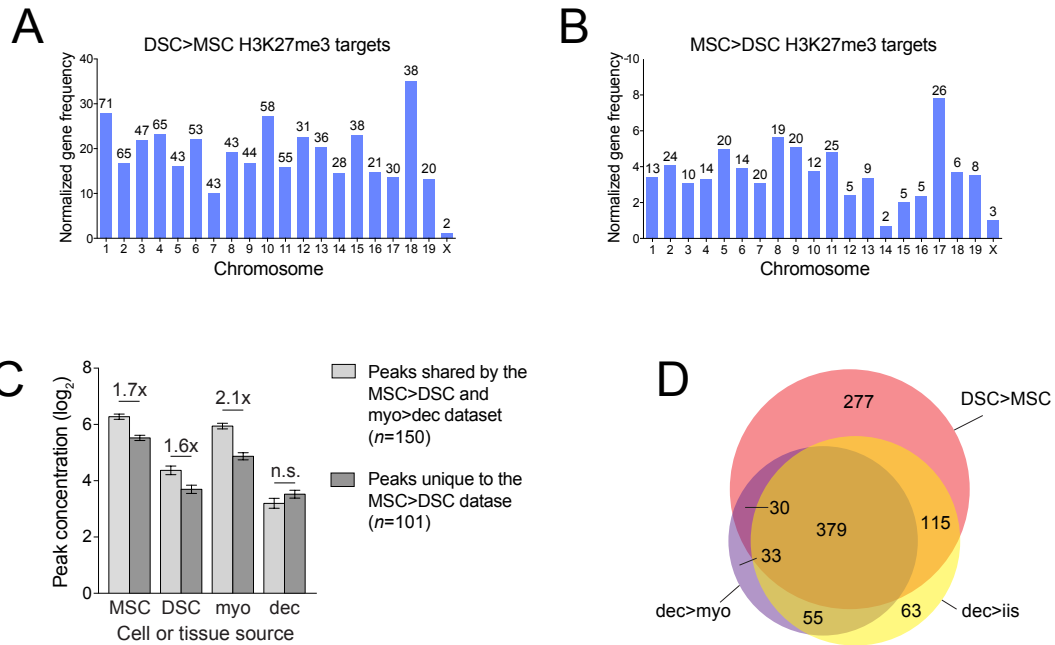
File contains:

Supplemental Figures 1-10

Supplemental References

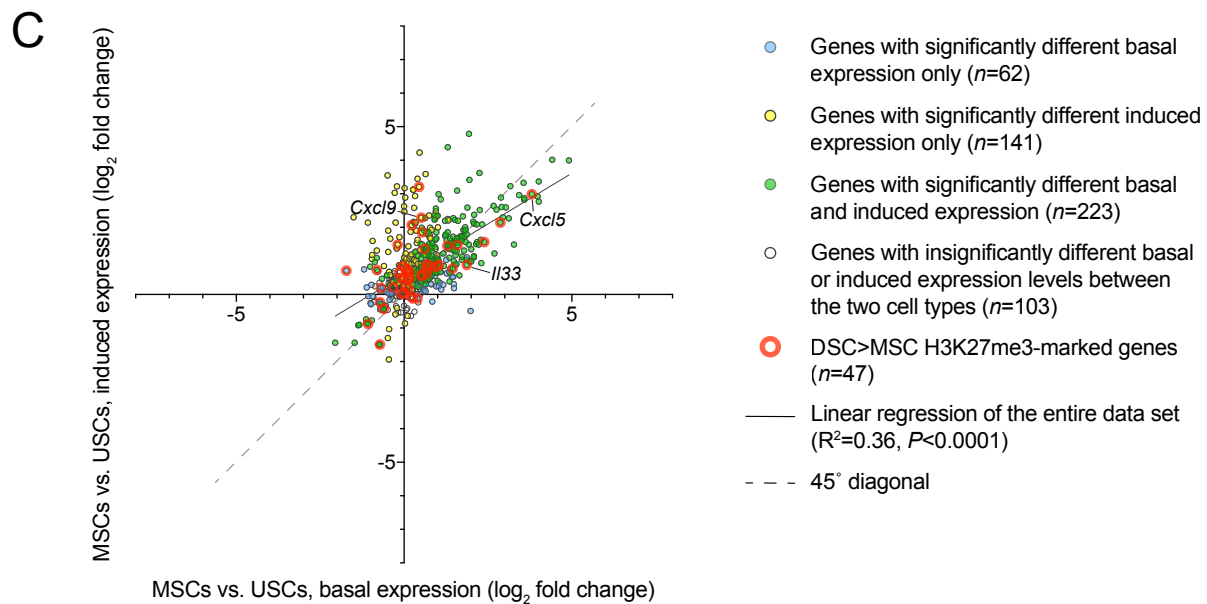
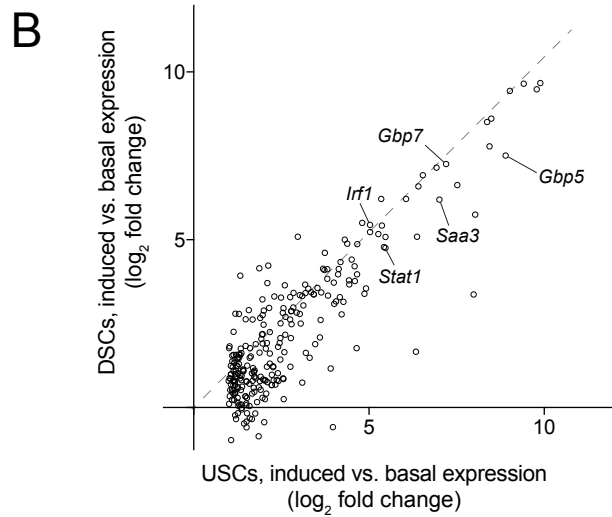
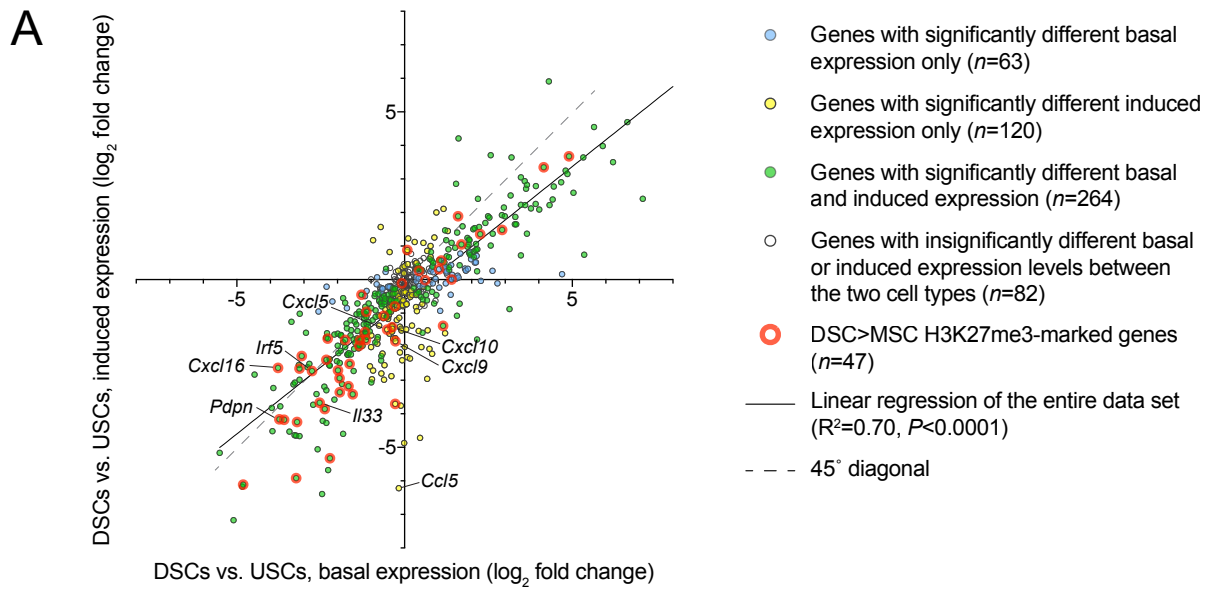
Notes on Supplemental Tables 1-6

Supplemental Tables 7&8

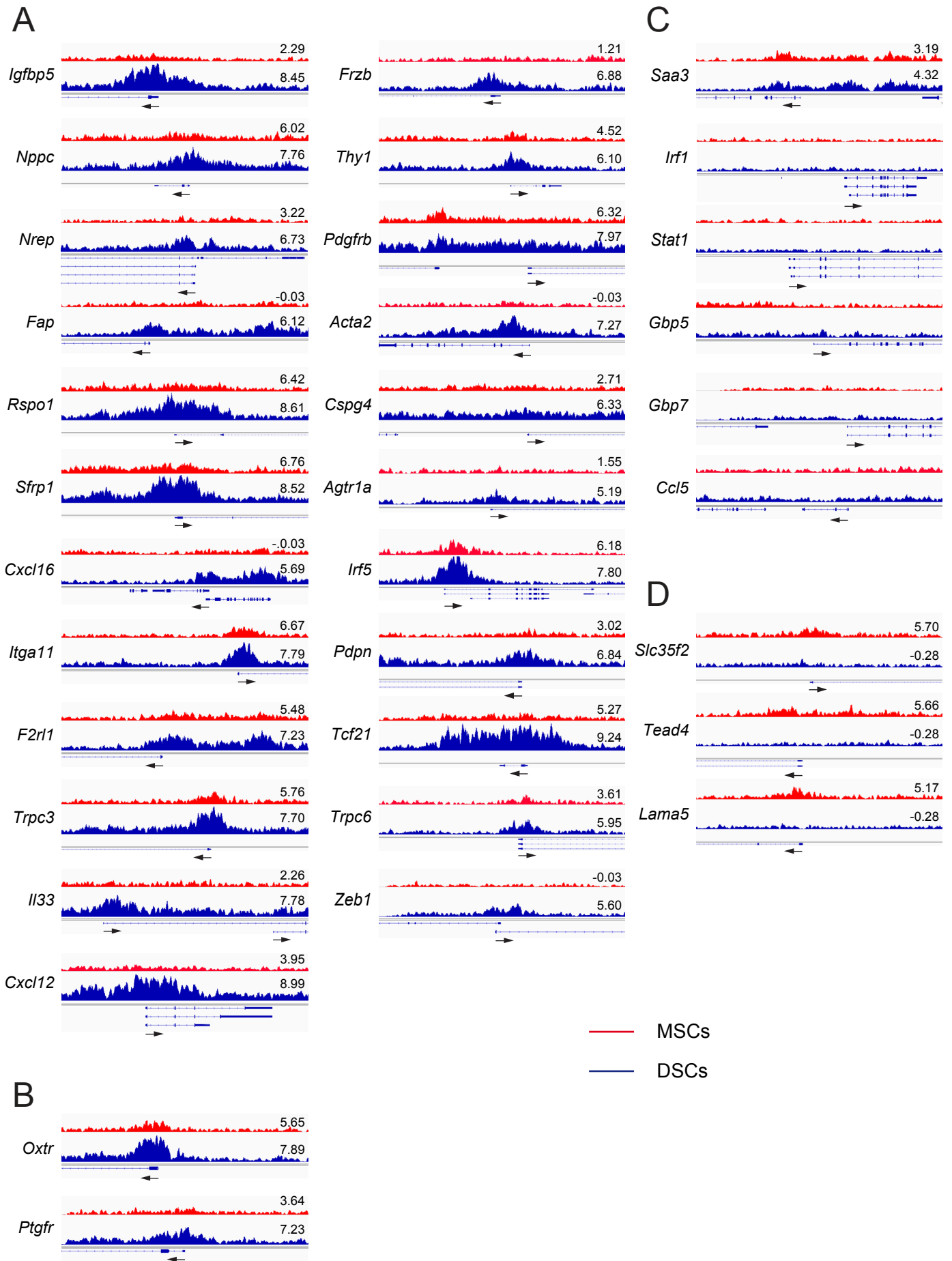


Nancy *et al.*, Supplemental Figure 1

Supplemental Figure 1. Additional analysis of H3K27me3 generation in the post-implantation uterus. (A, B) Chromosome frequency distribution of DSC>MSC- (A) and MSC>DSC- (B) associated genes, normalized to their frequency on the X chromosome. The absolute number of marked genes on each chromosome is indicated; total protein coding gene number per chromosome was calculated from <http://www.informatics.jax.org/downloads/reports/index.html#marker>. The frequency of marked genes on the X chromosome in both cases was significantly lower than their frequency on autosomes ($P<0.0001$; one-sample *t*-test). While this dual observation raises the possibility that DSC>MSC- and MSC>DSC-marked genes are underrepresented on the X chromosome, it is more likely the technical consequence of the abundance and thus interfering effect of H3K27me3 on the inactive X. (C) Absolute concentrations of MSC>DSC peaks in stromal cell and whole tissue layer extracts (mean \pm SEM). Significant differences are shown (unpaired *t*-test; n.s., not significant). The pattern of average peak concentrations of shared versus unique MSC>DSC peaks across different cells and tissues mirrored that of DSC>MSC peaks (Figure 1D), thus making the parallel case that some MSC>DSC peaks were undetectable as differentially enriched between tissue layers due to the compounded effects of their low concentration and interference from the non-stromal cell components of dec extracts. (D) Venn diagram showing the degree of overlap between DSC>MSC, dec>myo and dec>iis peak sets, complementing the analysis shown in Figure 1, E-F. Consistent with *de novo* peak accrual in the decidua, dec>iis peak sets showed a high degree of overlap with both DSC>MSC and dec>myo peak sets. (E-I) EZH2 immunostaining of pregnant uteri from E7.5 to E17.5. E10.5-17.5 embryos were removed prior to embedding. The slides were co-stained with antibodies to CK8 (not shown for clarity in the black and white images) to identify cells and structures. In contrast to the uniform decidual expression of EZH2 on E6.5 (Figure 1I), decidual staining was less uniform on E7.5, and by E10.5 was greatly reduced (E-F). On E7.5, EZH2 expression was apparent mainly in the mesometrial half of the decidua and in the overlying myometrium at the mesometrial pole of the uterus (m). In this area, the myometrium is starting to develop into the metrial gland (mg), a structure comprised of stromal cells and NK cells interspersed between strands of smooth muscle (and dissected as part of the myometrium). EZH2 expression in the metrial gland continued through E12.5 and then subsided, but was otherwise undetectable in the myometrium. EZH2 was also expressed at high levels within trophoblast giant cells (some indicated with arrowheads), in cells scattered throughout the placental labyrinth (lab), and in the trophoblasts that invade the mesometrial decidua in late gestation (I, corresponding to the bracketed area in h). CK8 positivity identifies these latter cells as trophoblasts; note that the surrounding decidual stromal cells are negative for EZH2. Intermediate expression was also detected in uterine epithelial cells. The spongiotrophoblast layer of the placenta (spg) showed non-specific staining associated with the plasma membrane. Images are representative of at least $n=3$ implantation sites from at least $n=3$ mice per time point.

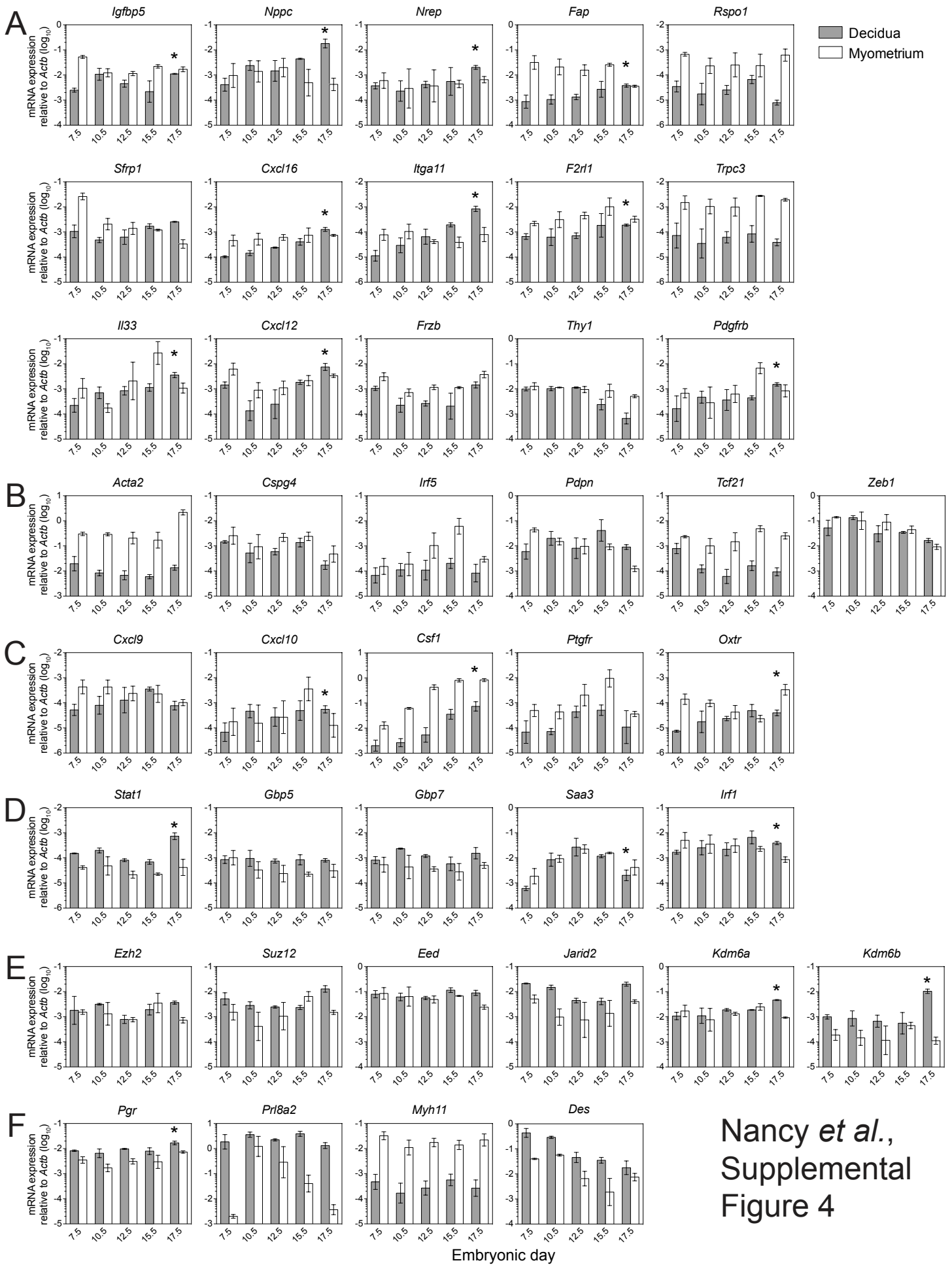


Supplemental Figure 2. Characteristics of inflammatory target gene expression in DSCs, USCs, and MSCs. USCs are the stromal cells isolated from the uteri of progesterone (P4)-treated virgin mice and consist of roughly equal proportions of ESCs and the stromal cells of the overlying (non-growing) myometrium (1). They provide a baseline for gene expression in the uterus under a pregnancy-like hormonal state but independent of the formation and growth of implantation sites. Inflammatory targets were defined as protein coding genes whose transcripts were significantly ($P_{adj}<0.05$) induced more than 2-fold in USCs following 6 h of exposure to $TNF\alpha+IFN\gamma$ (Supplemental Table 4). (A) Fold difference between DSCs and USCs in the induced mRNA expression level of each inflammatory target plotted against its fold difference in basal expression. The extent to which a gene has similar basal expression in the two cell types, independent of any difference in its inducibility (the fold increase in expression after $TNF\alpha+IFN\gamma$ treatment), can be seen through its proximity to the y -axis. *Ccl5* (indicated) is a prime example of a gene with a pure (and severe) inducibility defect in DSCs. Conversely, the extent to which a gene has a similar degree of inducibility in both cell types can be seen through its proximity to the 45° diagonal. Gene inducibility *per se* was on average about 35% less in DSCs, as indicated by the y -intercept of the linear regression (-0.62 ± 0.04 [best-fit value \pm SEM]). There was a strong over-representation of targets that were expressed at significantly lower levels in DSCs compared to USCs after $TNF\alpha+IFN\gamma$ stimulation (271 compared to 110 expected by chance alone, $P<0.00001$), to various extents the result of lower basal expression and/or impaired inducibility. The identity of several DSC>MSC marked genes are indicated; the complete set is shown in Supplemental Table 4. (B) Inducibility of the $n=258$ inflammatory target genes with unchanged or higher mRNA levels in DSCs compared to USCs after $TNF\alpha+IFN\gamma$ treatment. The degree of concordant inducibility of a gene in the two cell types is evident through a point's proximity to the 45° diagonal. Genes analyzed elsewhere in this study are indicated. (C) Fold difference between MSCs and USCs in the induced mRNA expression level of each inflammatory target plotted against its fold difference in basal expression. Gene inducibility *per se* was on average about 1.5-fold more in MSCs, as indicated by the y -intercept of the linear regression (0.59 ± 0.04). Also note the skewing towards higher basal expression in MSCs. These observations are consistent with the intimate association between fibroblast activation and inflammation (2). One gene so affected was *Csfl* (Supplemental Table 3), potentially explaining its upregulation with myometrial growth (3).

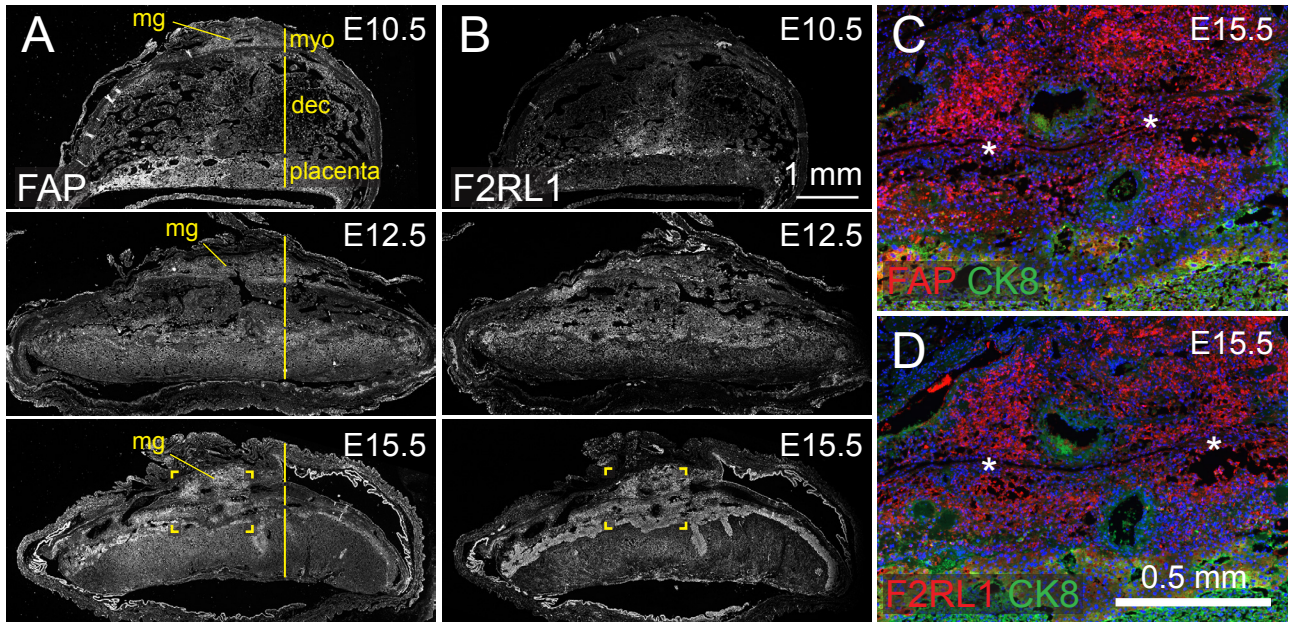


Nancy *et al.*, Supplemental Figure 3

Supplemental Figure 3. H3K27me3 tracks on select loci in DSCs and MSCs. Pileups from the $n=3$ independent replicates are shown. Each track is 25 kb and the TSS with direction of transcription is indicated (arrow). The \log_2 concentration for each called H3K27me3 peak is also indicated; lack of this information indicates that there was no called peak overlapping or less than 5 kb upstream of the TSS. The genes are grouped as follows: (A) fibroblast activation/myofibroblast inducers and markers with elevated H3K27me3 in DSCs; (B) parturition-inducing hormone receptors with elevated H3K27me3 in DSCs; (C) inflammatory targets lacking H3K27me3 enrichment in DSCs (see Supplemental Figure 2); (D) Examples of the top three MSC>DSC H3K27me3 targets with known gene function.

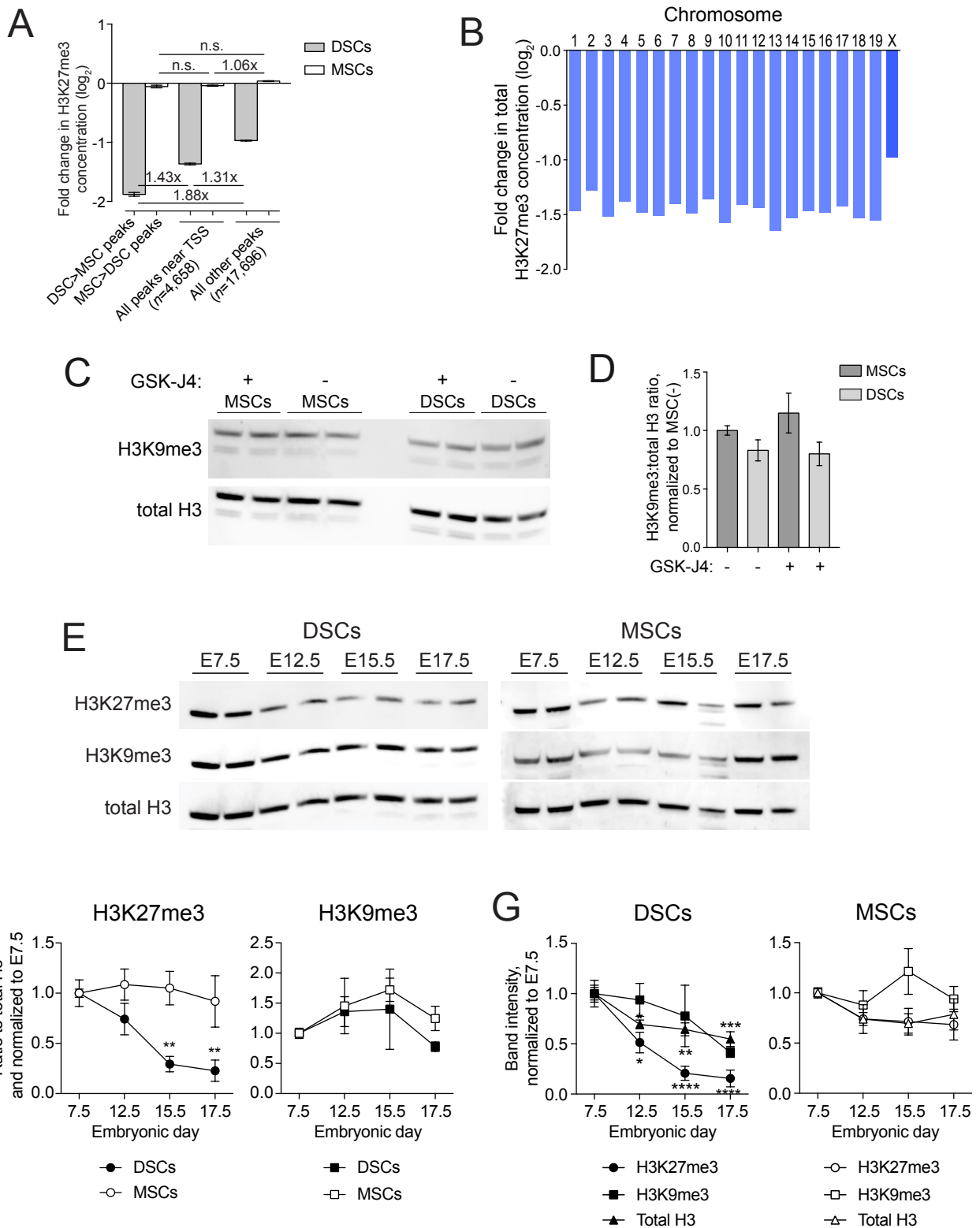


Supplemental Figure 4. Whole tissue layer qRT-PCR analysis of uterine gene expression. Data show mean±SD of $n=3$ mice/group. Unpaired t -tests were used to compare expression in the E17.5 decidua to the E7.5 decidua (*, upregulated transcript levels on E17.5, $P<0.05$). (A) The set of 15 fibroblast activation markers ranked the top half of Figure 3E. (B) Several additional fibroblast activation markers listed in the bottom half of Figure 3E. (C) Additional DSC>MSC H3K27me3 target genes of interest (*Cxcl9*, *Cxcl10*, *Csf1*, *Ptgfr*, *Oxtr*) (D) Inflammatory targets that lack H3K27me3 enrichment in DSCs. These markers were chosen for analysis based upon an RNA-Seq analysis demonstrating that they are highly (and similarly) inducible in USCs and DSCs by TNF α +IFN γ (Supplemental Figure 2B). (E) Genes (*Ezh2*, *Suz12*, *Eed* and *Jarid2*) encoding the main PRC2 complex components, as well as *Kdm6a* and *Kdm6b* encoding the two known H3K27me3 demethylases KDM6A and KDM6B. (F) Decidua and myometrial markers. *Pgr* encodes the progesterone receptor, *Pr18a2* encodes the DSC marker Dtrpr, *Myh11* encodes the smooth muscle marker myosin heavy chain 11, *Des* encodes the cytoskeletal protein desmin, which is expressed by both smooth muscle cells and DSCs.



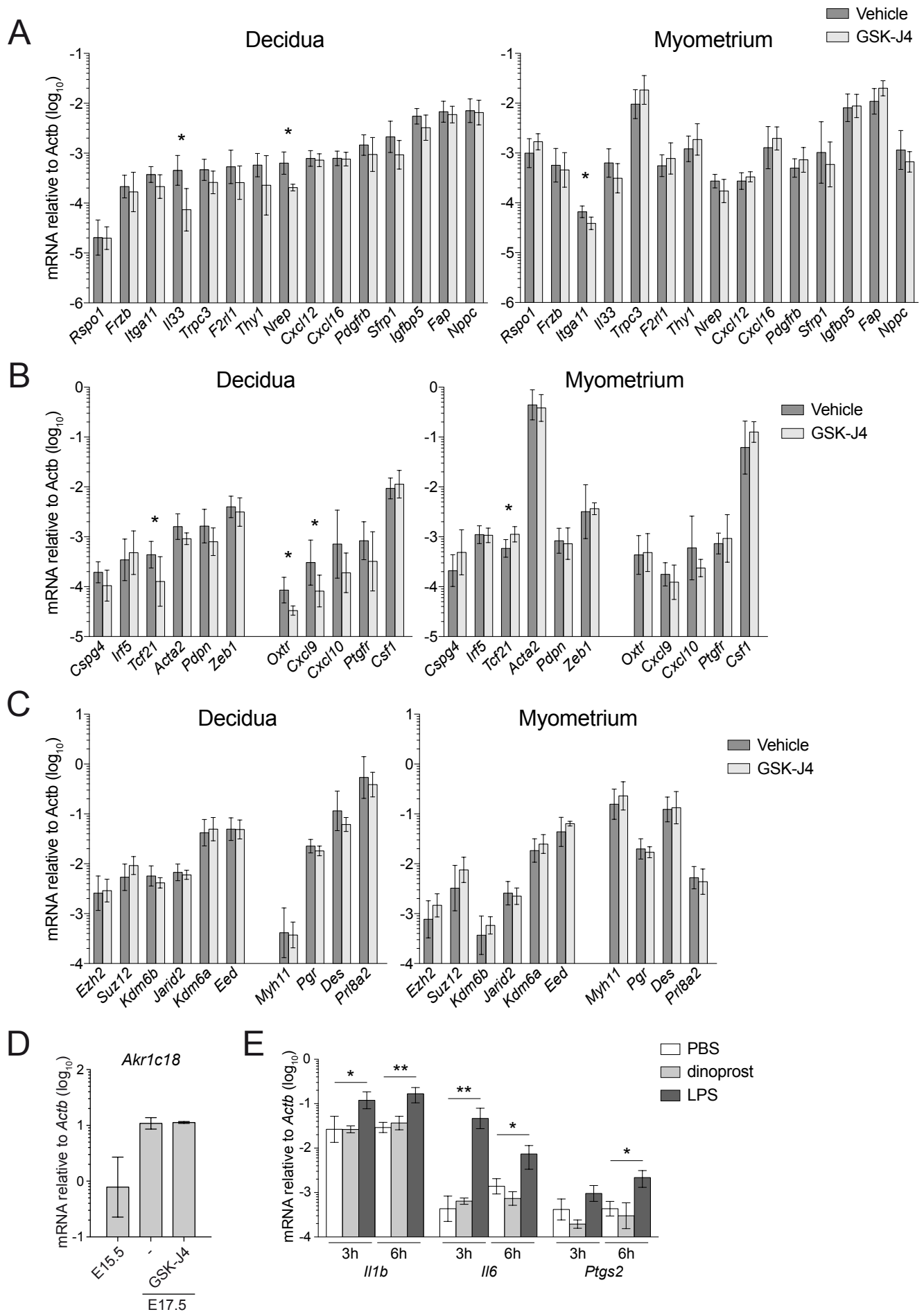
Nancy *et al.*, Supplemental Figure 5

Supplemental Figure 5. Immunofluorescence detection of FAP and F2RL1 (also called PAR2) in the second half of gestation. Sections were co-stained for CK8 to identify cells and structures (not shown for clarity in the black and white images; A, B). Asterisks in the close-ups of the bracketed areas indicate the strand of smooth muscle demarcating the border between the metrial gland (mg) and decidua (C, D). Note that FAP and F2RL1 are expressed by DSCs as well as by the non-smooth muscle stromal cells of the metrial gland. Images are representative of 3 implantation sites per mouse and $n=3$ mice per time point.



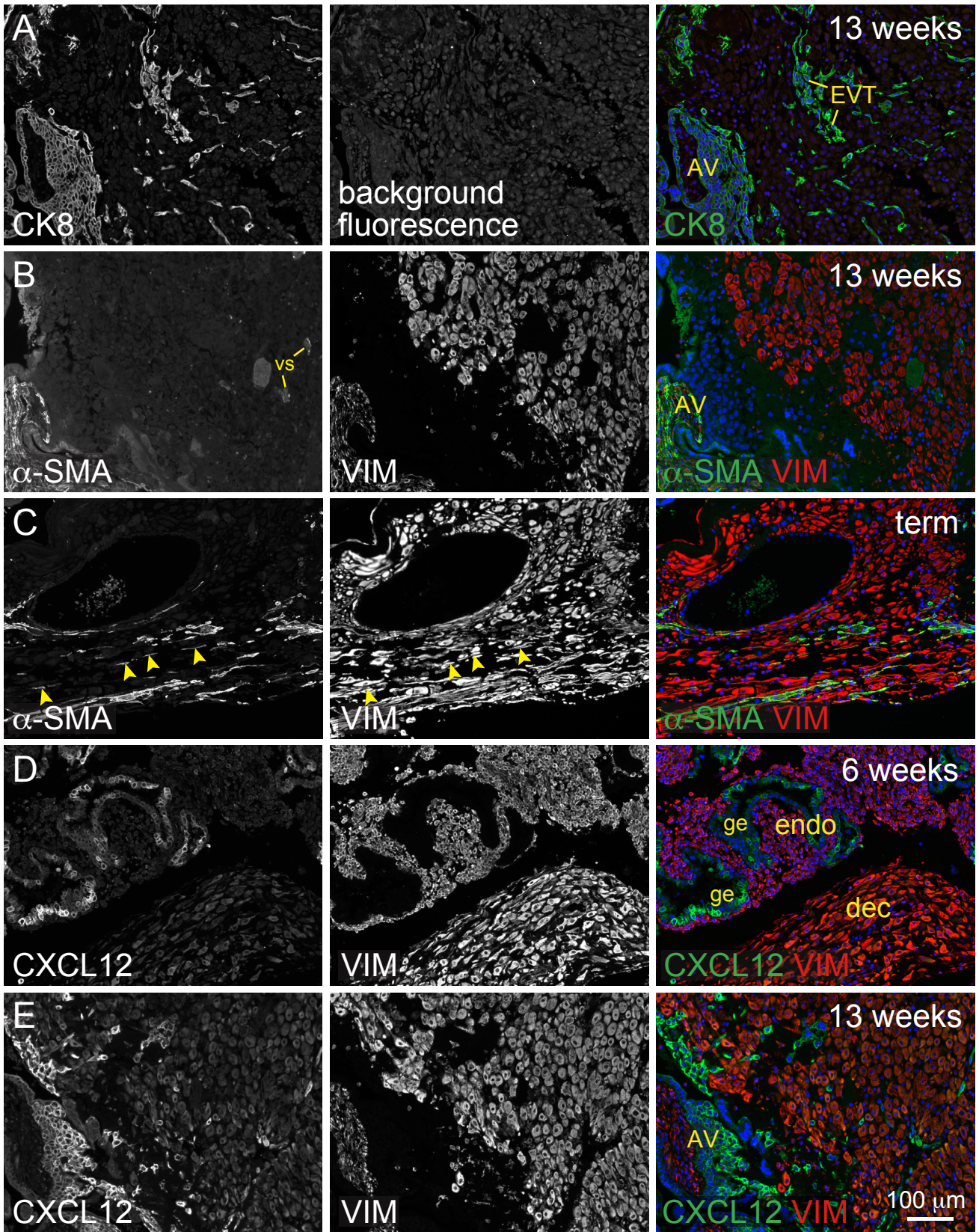
Nancy *et al.*, Supplemental Figure 6

Supplemental Figure 6. Further analysis of H3K27me3 dynamics in DSCs and MSCs with advancing gestation. (A, B) Non-uniform H3K27me3 peak loss in DSCs is apparent both within and between chromosomes. (A) Average fold changes in peak concentration from E7.5 to E15.5 for the indicated peak categories. Since DSC>MSC peaks were undetectable on the X chromosome (Supplemental Figure 1), this analysis considered autosomes only. Significant differences were determined by one-way ANOVA followed by Tukey's multiple comparison test (DSCs: $P<0.0001$; MSCs: $P<0.0001$). Significant differences (all $P<0.0001$) are indicated. H3K27me3 loss in DSCs was seen with DSC>MSC peaks, to a lesser extent with all peaks near TSSs, and to a still lesser extent to all other peaks. Peak concentrations were virtually unchanged in MSCs. (B) Fold changes from E7.5 to E15.5 in the summated H3K27me3 peak concentrations in DSCs on each chromosome. Loss from X chromosomes was significantly less than from the aggregate set of autosomes ($P<0.0001$, one-sample *t*-test), consistent with relative sparing of the inactive X. (C) Western blot of H3K9me3 and total H3 in MSCs and DSCs isolated from E15.5 mice treated with GSK-J4 or vehicle (-) and cultured for 24 h. (D) Quantified H3K9me3 levels normalized to total H3. Data show mean \pm SEM from $n=2$ samples per group. The average ratio of H3K9me3 to total H3 for the MSC samples from vehicle-treated mice was set to 1.0. No differences were statistically significant ($P=0.23$, one-way ANOVA). (E, F) Representative western blots (E) and quantified levels of H3K27me3 and H3K9me3, as normalized to total H3 (F) for DSCs ($n=6$ samples/group; 3 sets of blots) and MSCs ($n=4$ samples per group; 2 different sets of blots) isolated at the indicated days of gestation and cultured for 24 h. Data show mean \pm SEM. For each set, the average ratio of the modification to total H3 at E7.5 was set to 1.0. Results of one-way ANOVA followed by Tukey's multiple comparison test performed on each set are as follows: DSCs: $P=0.0005$; **, $P<0.005$ compared to E7.5; MSCs: $P=0.91$. (G) Quantified H3K27me3, H3K9me3, and total H3 levels independently plotted. For each set, the average band intensity for the E7.5 samples was set to 1.0. Results of one-way ANOVA performed on each set are as follows: DSCs, total H3: $P=0.0003$; DSC, H3K27me3: $P<0.0001$; DSC, H3K9me3 $P=0.13$; MSC, total H3: $P=0.31$; MSC H3K27me3: $P=0.20$; MSC H3K9me3: $P=0.45$. *, $P<0.05$, **, $P<0.005$, ***, $P<0.0005$, ****, $P<0.0001$ compared to E7.5. Relative to total H3 levels, which themselves showed a modest but reproducible decline with advancing gestation, H3K27me3 levels in DSCs were 70-80% lower on E15.5 and E17.5 as compared to E7.5, but unchanged on E12.5. H3K27me3:total H3 ratios remained constant in MSCs, as did total H3 levels, while H3K9me3 levels:total H3 ratios remained constant in both cell types.



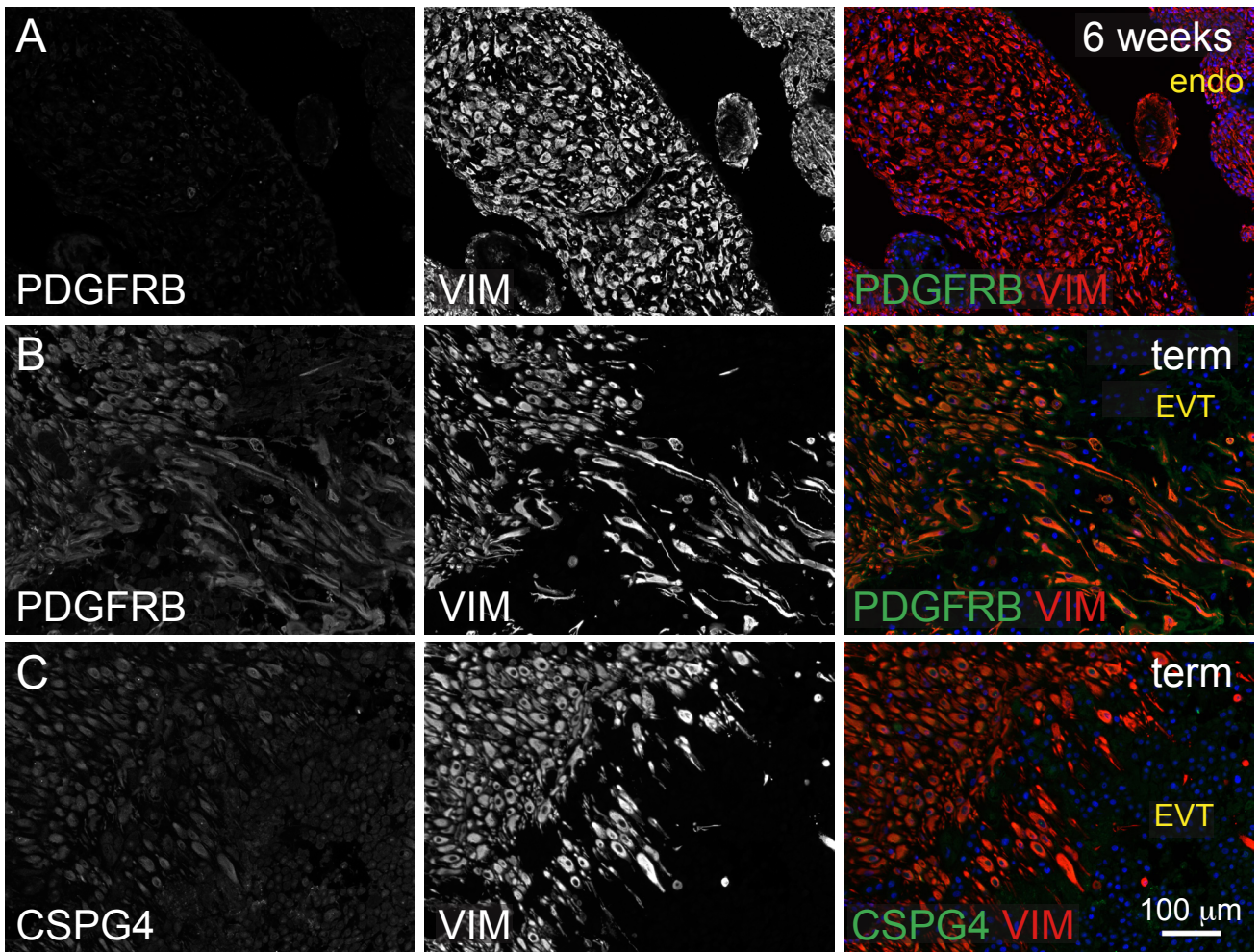
Nancy *et al.*, Supplemental Figure 7

Supplemental Figure 7. Additional effects of GSK-J4 and dinoprost. (A-C) Effect of GSK-J4 on gene expression in the E17.5 decidua and myometrium. Data show mean±SD of $n=6$ mice/group; asterisks indicate statistically significant differences ($P<0.05$, unpaired t -test). (A) The 15 fibroblast activation/myofibroblast markers with H3K27me3 enrichment in E7.5 DSCs versus MSCs (i.e., H3K27me3 DSC>MSC targets) listed in the top portion of Figure 3E; (B) additional fibroblast activation/myofibroblast markers that are also H3K27me3 DSC>MSC targets (left portion of graphs; see bottom portion of Figure 3E), as well as additional H3K27me3 DSC>MSC targets of interest (right portion of graphs); (C) genes encoding PRC2 components, H3K27me3 demethylases, decidual and myometrial markers, and *Pgr*. (D) Effect of GSK-J4 on ovarian 20 α -hydroxysteroid dehydrogenase mRNA expression (encoded by *Akr1c18*). Data show mean±SD of $n=3-5$ mice per group. Data from untreated E15.5 mice are included to illustrate the upregulation of *Akr1c18* near term. (E) Contrasting effects of dinoprost and LPS on lung inflammation. Virgin females were injected intraperitoneally with PBS, 50 μ g LPS or 60 μ g dinoprost and sacrificed at the indicated time points. Lung RNA was analyzed by qRT-PCR. Data show mean±SD of $n=3$ mice/group. *, $P<0.05$; **, $P<0.005$ by unpaired t -test.



Nancy *et al.*, Supplemental Figure 8

Supplemental Figure 8. Additional α -SMA and CXCL12 immunostaining of the human endometrium and decidua. Images are representative of $n=5$ specimens per time point. Specimens at 6 and 13 weeks were from elective terminations. (A, B, E) Neighboring sections of a 13 week specimen at the site where an anchoring villous (AV) of the placenta has attached to the decidua. (A) CK8 staining identifies trophoblasts, including EVT. (B) α -SMA/VIM staining. Note the complete lack of α -SMA expression by DSCs; only decidual vascular structures (vs) and the villous stroma (left lower corner) are α -SMA⁺. (C) α -SMA/VIM staining at term. Note the α -SMA⁺ VIM⁺ cells with spindly morphology (arrowheads) that do not appear to be associated with vascular structures. This morphology suggests contractile activity and contrasts with other α -SMA⁺ VIM⁺ cells within the term basal plate that retain the plump morphology of DSCs (Figure 6B). (D) CXCL12/VIM staining at 6 weeks. Both the endometrium and decidua are negative for CXCL12, but the glandular epithelium is moderately positive. (E) CXCL12/VIM staining at 13 weeks. As in Figure 6C, note that EVTs express more CXCL12 than DSCs.

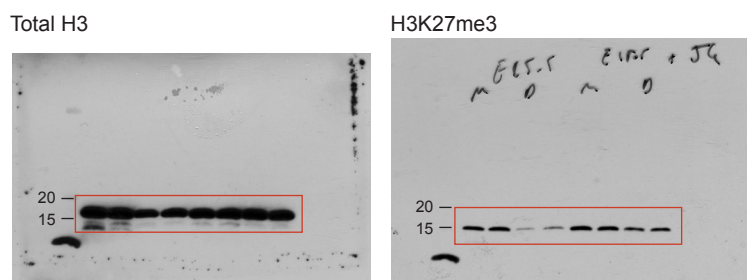


Nancy *et al.*, Supplemental Figure 9

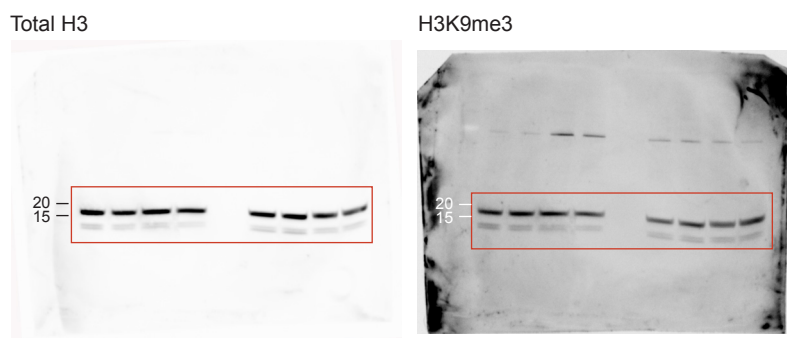
Supplemental Figure 9. PDGFRB and CSPG4 immunostaining of the human endometrium and decidua. Images are representative of $n=5$ specimens per time point. Specimens at 6 weeks were from elective terminations. (A, B) PDGFRB/VIM staining. Note the increased expression of PDGFRB in VIM⁺ cells at term contrasting with EVT_s, which are PDGFRB⁻. EVT_s were identified by cytokeratin 7 staining (not shown). (C) CSPG4 immunostaining. Note that VIM⁺ cells do not express CSPG4 above the background levels shared by EVT_s.

Full unedited gels

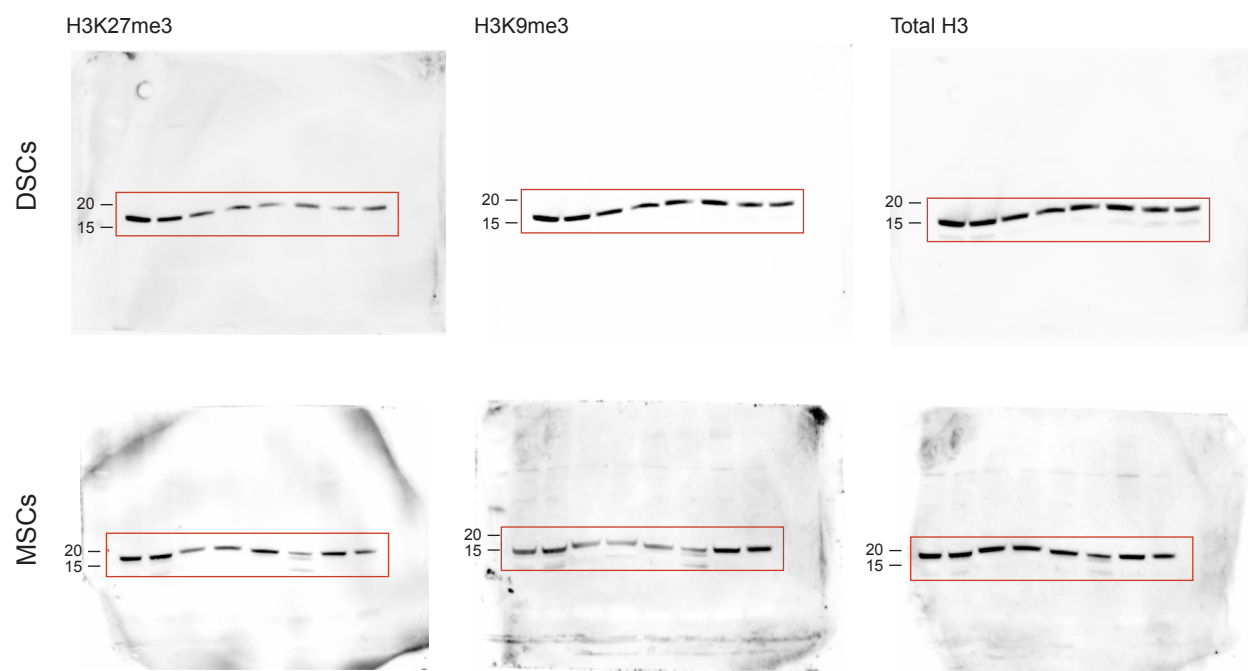
Figure 4C



Supplemental Figure 6C



Supplemental Figure 6E



SUPPLEMENTAL REFERENCES

1. Nancy P, Tagliani E, Tay CS, Asp P, Levy DE, and Erlebacher A. Chemokine gene silencing in decidual stromal cells limits T cell access to the maternal-fetal interface. *Science*. 2012;336(6086):1317-21.
2. Millar NL, O'Donnell C, McInnes IB, and Brint E. Wounds that heal and wounds that don't - The role of the IL-33/ST2 pathway in tissue repair and tumorigenesis. *Seminars in cell & developmental biology*. 2016.
3. Tagliani E, Shi C, Nancy P, Tay CS, Pamer EG, and Erlebacher A. Coordinate regulation of tissue macrophage and dendritic cell population dynamics by CSF-1. *J Exp Med*. 2011;208(9):1901-16.

NOTES ON SUPPLEMENTAL TABLES 1-6

Supplemental Table 1. Characteristics of DSC>MSC and MSC>DSC H3K27me3 peaks.

Notes: Duplicate peaks and genes are highlighted in yellow in columns B and V, respectively. These duplicates exist because some peaks have multiple associated genes and some genes have multiple associated peaks. The peaks are ranked based upon how much their concentrations diverge between DSCs and MSC. Data from whole tissues (dec, myo, iis) is also included. Peak concentrations (conc) are averages of $n=3$ independent replicates of DSCs, MSCs, dec, and iis samples and $n=2$ replicates of myo samples. The false discovery rate (FDR) for the \log_2 -fold change (\log_2FC) of each comparison was calculated based upon all the comparisons made for the dataset across all samples.

Supplemental Table 2. Characteristics of dec>myo, myo>dec, myo>iis, iis>myo, dec>iis, and iis>dec H3K27me3 peaks.

Notes: Duplicate peaks and genes are highlighted in yellow in columns B and V, respectively. These duplicates exist because some peaks have multiple associated genes and some genes have multiple associated peaks. The peaks are ranked based upon how much their concentrations diverge for the comparison indicated in the worksheet tab. In the dec>myo dataset, genes listed in red in column G are those that are also in the DSC>MSC dataset. In the myo>dec dataset, genes listed in red in column G are those that are also in the MSC>DSC dataset. In the iis>myo dataset, genes listed in red in column G are those that are also in the DSC>MSC dataset. Peak concentrations (conc) are averages of $n=3$ independent replicates of DSCs, MSCs, dec, and iis samples and $n=2$ replicates of myo samples. The false discovery rate (FDR) for the \log_2 -fold change (\log_2FC) of each comparison was calculated based upon all the comparisons made for the dataset across all samples.

Supplemental Table 3. RNA-Seq analysis of DSCs, MSCs, and USCs – total data set and all DSC>MSC H3K27me3 target genes.

Notes: Only protein coding genes are listed. Genes highlighted in red are DSC>MSC H3K27me3 targets. Fold changes in H3K27me3 peak concentrations for these loci are listed at the right, as are those for genes that are MSC>DSC H3K27me3 targets. The genes are ranked first by H3K27me3 status, then by the fold difference in RNA expression between DSCs and USCs. The tables show both basal mRNA expression in the three cell types (DSCs, USCs, and MSCs), and (for consistency between Supplemental Tables 3 and 4) induced mRNA expression in these cell types after $TNF\alpha+IFN\gamma$ treatment. Normalized counts are averages of the $n=3$ independent replicates of each sample type. The P_{adj} value for the \log_2 -fold change (\log_2FC) of each comparison was calculated based upon all the comparisons made for the dataset across all samples.

Supplemental Table 4. RNA-Seq analysis of DSCs, MSCs, and USCs – genes with significantly different expression between DSCs and USCs, and between MSCs and USCs; also, inflammatory targets.

Notes: The first four tabs correspond to the four quadrants of Figure 3D, and list all the genes shown in each quadrant. The genes are by ranked by the fold difference in RNA expression between DSCs and MSCs. The last tab lists the $n=529$ inflammatory target genes defined as those that are significantly ($P_{\text{adj}} < 0.05$) upregulated in USCs more than 2-fold after $\text{TNF}\alpha + \text{IFN}\gamma$ treatment. The genes are by ranked by their fold induction in USCs. For all tables, genes highlighted in red are DSC>MSC H3K27me3 targets. Fold changes in H3K27me3 peak concentrations for these loci are listed at the right, as are those for genes that are MSC>DSC H3K27me3 targets. All tables also show both basal mRNA expression in the three cell types (DSCs, USCs, and MSCs), and (for consistency between Supplemental Tables 3 and 4) induced mRNA expression in these cell types after $\text{TNF}\alpha + \text{IFN}\gamma$ treatment. Normalized counts are averages of the $n=3$ independent replicates of each sample type. The P_{adj} value for the \log_2 -fold change ($\log_2\text{FC}$) of each comparison was calculated based upon all the comparisons made for the dataset across all samples.

Supplemental Table 5. Changes in gene expression between E7.5 and E15.5, stratified by H3K27me3 status in DSCs.

Notes: Each tab lists genes associated with the category of H3K27me3 status indicated. Genes in the first (H3K27me3 DSC>MSC target genes only), second (all genes with peaks), third (all genes without peaks), and fourth tab (genes for which H3K27me3 levels did not significantly change between E15.5 and E7.5 DCSs) are ranked in alphabetical order by gene name. Otherwise, the genes are by ranked by the fold difference their associated H3K27me3 level between E15.5 and E7.5 DSCs. All tables show basal mRNA expression in the four cell types (average normalized counts of the $n=3$ replicates), key comparisons of RNA expression, average H3K27me3 peak concentrations ($n=3$ replicates) and key comparisons of H3K27me3 peak concentrations. For all tabs, genes highlighted in red are DSC>MSC H3K27me3 targets.

Supplemental Table 6. Changes in DSC>MSC and MSC>DSC H3K27me3 peak concentrations with advancing gestation.

Notes: Duplicate peaks and genes are highlighted in yellow in columns B and column V, respectively. These duplicates exist because some peaks have multiple associated genes and some genes have multiple associated peaks. The peaks are ranked based upon how much their concentrations diverge for the comparison indicated in the worksheet tab. Peak concentrations (conc) are averages of $n=3$ independent replicates of DSCs, MSCs, dec, and iis samples and $n=2$ replicates of myo samples. The false discovery rate (FDR) for the \log_2 -fold change ($\log_2\text{FC}$) of each comparison was calculated based upon all the comparisons made for the dataset across all samples.

Nancy *et al.*, Supplemental Table 7

Treatment	Mouse #	Day of delivery/ pregnancy termination	Pups	Viable pups	Notes
None	1	E18.5	6	6	All pups delivered
	2	E18.5	7	7	All pups delivered
	3	E18.5	8	8	All pups delivered
	4	E18.5	7	7	All pups delivered
	5	E18.5	7	7	All pups delivered
	6	E18.5	4	4	All pups delivered
	7	E18.5	7	7	All pups delivered
	8	E18.5	9 (Total=55)	9 (Total=55; 100.0%)	All pups delivered
GSK-J4	1	E18.5	8	8	All pups delivered
	2	E18.5	6	6	All pups delivered
	3	E19.0	8	7	All pups delivered
	4	E19.0	6	6	All pups delivered
	5	E19.0	5	5	All pups delivered
	6	E19.0	6	6	All pups delivered
	7	E19.5	7	7	All pups delivered
	8	E19.5	8 (Total=54)	8 (Total=54; 98.1%)	All pups delivered
P4	1	E19.0	9	9	All pups delivered
	2	E19.5	7	0	All pups delivered
	3	E20.5	7	0	All pups delivered
	4	E20.5	7	7	All pups delivered
	5	E20.5	8	8	All pups delivered
	6	E21.0	8	5	All pups delivered
	7	E21.5	7	0	All pups delivered
	8	E21.5	10 (Total=63)	0 (Total=29; 46.0%)	All pups delivered
P4 + vehicle	1	E19.0	9	9	All pups delivered
	2	E19.0	7	7	All pups delivered
	3	E19.5	9	8	All pups delivered
	4	E20.5	nd ^A	0	All pups delivered
	5	E20.5	9	0	All pups delivered
	6	E21.0	8	0	All pups delivered
	7	E21.5	9	0	All pups delivered
	8	E23.5	9 (Total=60+nd)	0 (Total=24; 40.0%)	No delivery, mother sacrificed in distress
P4 + GSK-J4	1	E19.5	9	0	All pups delivered
	2	E20.5	4+nd	0	All pups delivered
	3	E21.5	8	0	All pups delivered
	4	E21.5	6	0	All pups delivered
	5	E22.5	7	0	No pups delivered, mother sacrificed in distress
	6	E22.5	3+nd	0	No pups delivered, mother sacrificed in distress
	7	E23.5	6	0	No pups delivered, mother sacrificed in distress
	8	E24.5	6+nd (Total=36+nd)	0 (Total=0; 0.0%)	No pups delivered, mother sacrificed in distress
Dinoprost	1	E17.5	6+nd	0	All pups delivered
	2	E17.5	2+nd	0	All pups delivered
	3	E17.5	5+nd	0	All pups delivered
	4	E17.5	nd	0	All pups delivered
	5	E17.5	7	0	All pups delivered
	6	E17.5	8	0	All pups delivered
	7	E17.5	8 (Total=23+nd)	0 (Total=0; 0.0%)	All pups delivered
Dinoprost + P4	1	E17.5	8	2	No pups delivered
	2	E17.5	7	3	No pups delivered
	3	E17.5	7	2	No pups delivered
	4	E17.5	8	2	No pups delivered
	5	E17.5	9	3	No pups delivered
	6	E17.5	8 (Total=47)	1 (Total=13; 27.7%)	No pups delivered
P4	1	E17.5	8	8	No pups delivered
	2	E17.5	8	8	No pups delivered
	3	E17.5	4	4	No pups delivered
	4	E17.5	5	5	No pups delivered
	5	E17.5	8	8	No pups delivered
	6	E17.5	7 (Total=40)	7 (Total=40; 100.0%)	No pups delivered
Dinoprost + GSK-J4	1	E17.5	7	6	No pups delivered
	2	E17.5	6	6	No pups delivered
	3	E17.5	8	6	No pups delivered
	4	E17.5	6	4	No pups delivered
	5	E17.5	9	7	No pups delivered
	6	E17.5	8	8	No pups delivered
	7	E17.5	11 (Total=55)	10 (Total=47; 85.5%)	No pups delivered
GSK-J4	1	E17.5	7	7	No pups delivered
	2	E17.5	6	6	No pups delivered
	3	E17.5	10	10	No pups delivered
	4	E17.5	7	7	No pups delivered
	5	E17.5	7	7	No pups delivered
	6	E17.5	7	7	No pups delivered
	7	E17.5	5	5	No pups delivered
	8	E17.5	9 (Total=51)	9 (Total=51; 100.0%)	No pups delivered

^And, not able to be accurately determined, however pups (or additional pups) were inferred to exist either because of the existence of unaccounted for body parts, or due to evidence of additional implantation sites beyond the number of recovered pups.

Nancy *et al.*, Supplemental Table 8

Antibody	Source	Use
Rat anti-mouse CD102 (clone 3C4)	Biologend	Stromal cell purification
Rat anti-mouse CD326 (clone G8.8)	Developmental Studies Hybridoma Bank	Stromal cell purification
Ter119 microbeads, mouse	Miltenyi Biotec; 130-049-901	Stromal cell purification
CD45 microbeads, mouse	Miltenyi Biotec; 130-052-301	Stromal cell purification
Goat anti-rat IgG microbeads	Miltenyi Biotec; 130-048-501	Stromal cell purification
FITC-conjugated rat anti-mouse CD102 (clone 3C4)	Biologend	Flow cytometry for stromal cell purity
PE-Cy7-conjugated rat anti-mouse CD45 (clone 30-F11)	Biologend	Flow cytometry for stromal cell purity
Rabbit anti-mouse H3K27me3 (polyclonal IgG)	Millipore; 07-449	ChIP-Seq assays and western blots; 1:10000 dilution for western blots
Rabbit anti-mouse H3K9me3 (polyclonal IgG)	Abcam; ab8898	Western blots; 1:10000 dilution
Rabbit anti-mouse Histone H3 (polyclonal IgG)	Abcam; ab1791	Western blots; 1:5000 dilution
Goat anti-rabbit IgG HRP-conjugated	Abcam; ab6721	Western blots; 1:10000 dilution
Rat anti-mouse cytokeratin 8 (clone Troma-1)	Developmental Studies Hybridoma Bank	Tissue immunostaining (mouse) Ag retrieval: Tris-EDTA, citrate, trypsin; 1:100 dilution
Rabbit anti-mouse Ezh2 (clone SP129)	Acris Origena	Tissue immunostaining (mouse) Ag retrieval: Tris-EDTA; 1:1000 dilution
Rabbit anti-mouse F2RL1 (PAR2) (clone EPR13675)	Abcam	Tissue immunostaining (mouse) Ag retrieval: Tris-EDTA; 1:1000 dilution
Rabbit anti-mouse FAP (polyclonal IgG)	Abcam; ab28244	Tissue immunostaining (mouse) Ag retrieval: citrate; 1:1000 dilution
Biotin-conjugated rat anti-mouse macrophage F4/80 (clone C1:A3-1)	Cedarlane	Tissue immunostaining (mouse); Ag retrieval: trypsin; 1:200 dilution
Rabbit anti-GFP (polyclonal IgG)	Life Technologies; A-11122	Tissue immunostaining (mouse) Ag retrieval: trypsin; 1:1000 dilution
Rabbit anti-human Vimentin (polyclonal IgG)	Invitrogen; PA5-27231	Tissue immunostaining (human) Ag retrieval: citrate; 1:1000 dilution
Mouse anti-human α -SMA (clone 1A4)	Life Technologies	Tissue immunostaining (human) Ag retrieval: citrate; 1:100 dilution
Mouse anti-human CSPG4 (NG2/MCSP) (clone LHM 2)	Novus Biologicals	Tissue immunostaining (human) Ag retrieval: citrate; 1:50 dilution
Rabbit anti-human CK7 (clone EPR1619Y)	Abcam	Tissue immunostaining (human) Ag retrieval: citrate; 1:300 dilution
Mouse anti-human PDGFRB (clone 1E8)	LifeSpan Biosciences	Tissue immunostaining (human) Ag retrieval: citrate; 1:50 dilution
Mouse anti-human SDF-1 (clone MM0211-9N26)	Novus Biologicals	Tissue immunostaining (human) Ag retrieval: citrate; 1:1000 dilution
Donkey anti-rabbit IgG, HRP-conjugated	ThermoFisher Scientific	Tissue immunostaining; 1:200 dilution
Donkey anti-rabbit IgG, Alexa Fluor 488	ThermoFisher Scientific	Tissue immunostaining; 1:200 dilution
Donkey anti-rabbit IgG, Alexa Fluor 594	ThermoFisher Scientific	Tissue immunostaining; 1:200 dilution
Donkey anti-mouse IgG, Alexa Fluor 488	ThermoFisher Scientific	Tissue immunostaining; 1:200 dilution